

## Long-term changes in stratospheric age spectra in the 21st century in the Goddard Earth Observing System Chemistry-Climate Model (GEOSCCM)

Feng Li,<sup>1,2</sup> Darryn W. Waugh,<sup>3</sup> Anne R. Douglass,<sup>2</sup> Paul A. Newman,<sup>2</sup> Susan E. Strahan,<sup>1,2</sup> Jun Ma,<sup>4</sup> J. Eric Nielsen,<sup>2,5</sup> and Qing Liang<sup>1,2</sup>

Received 6 April 2012; revised 18 August 2012; accepted 24 September 2012; published 30 October 2012.

[1] In this study we investigate long-term variations in the stratospheric age spectra using a 21st century simulation with the Goddard Earth Observing System Chemistry-Climate Model (GEOSCCM). Our purposes are to characterize the long-term changes in the age spectra, and identify processes that cause the decrease of the mean age in a changing climate. Changes in the age spectra in the 21st century simulation are characterized by decreases in the modal age, the mean age, the spectral width, and the tail decay timescale throughout the stratosphere. Our analyses show that the decrease in the mean age is caused by two processes: the acceleration of the residual circulation that increases the young air masses in the stratosphere, and the weakening of the recirculation that leads to a decrease of the tail of the age spectra and a decrease of the old air masses. Weakening of the stratospheric recirculation is also strongly correlated with the increase of the residual circulation. One important result of this study is that the decrease of the tail of the age spectra makes an important contribution to the decrease of the mean age. Long-term changes in the stratospheric isentropic mixing are also investigated. Mixing increases in the subtropical lower stratosphere, but its impact on the age spectra is smaller than the increase of the residual circulation. The impacts of the long-term changes in the age spectra on long-lived chemical tracers are also investigated.

**Citation:** Li, F., D. W. Waugh, A. R. Douglass, P. A. Newman, S. E. Strahan, J. Ma, J. E. Nielsen, and Q. Liang (2012), Long-term changes in stratospheric age spectra in the 21st century in the Goddard Earth Observing System Chemistry-Climate Model (GEOSCCM), *J. Geophys. Res.*, 117, D20119, doi:10.1029/2012JD017905.

### 1. Introduction

[2] Coupled Chemistry-Climate Models (CCMs) consistently simulate an acceleration of the stratospheric circulation in the recent past and the 21st century [Butchart *et al.*, 2006, 2010]. The strengthening of the stratospheric circulation in a warming climate is reflected in two diagnostics: the increase of the mean meridional mass circulation [Butchart and Scaife, 2001; Butchart *et al.*, 2006, 2010; Li *et al.*, 2008; Garcia and Randel, 2008; McLandress and Shepherd, 2009] and the decrease of the mean age of stratospheric air [Austin and Li, 2006; Oman *et al.*, 2009; Butchart *et al.*, 2010]. These two diagnostics are strongly correlated [Austin and Li, 2006], but they have different physical meanings. The

mean meridional mass circulation, often approximated by the Transformed Eulerian Mean residual circulation, estimates the mean advection part of the stratospheric transport circulation [Andrews *et al.*, 1987]. In this paper the mean meridional mass circulation is referred to as the residual circulation, although it is also called the Brewer-Dobson circulation or diabatic circulation [e.g., Andrews *et al.*, 1987; Shepherd, 2002]. The mean age of air is the average time for an air parcel to be transported from the troposphere to a stratospheric sampling region. It is a measure of the strength of the stratospheric transport circulation. The mean age is determined not only by the residual circulation, but also by other processes such as isentropic mixing and recirculation [Waugh and Hall, 2002].

[3] There are very few observational studies to verify the simulated mean age changes. Engel *et al.* [2009] examined a long-term record of mean age of air derived from CO<sub>2</sub> and SF<sub>6</sub> measurements in the northern midlatitudes and found no significant trend in the last three decades, contrary to CCM simulations. However, Garcia *et al.* [2011] pointed out that the results of Engel *et al.* [2009] have serious caveats due to sparse sampling and the nonlinear growth rate of CO<sub>2</sub> and SF<sub>6</sub>. Nevertheless, there are still doubts on the model projected mean age changes.

<sup>1</sup>Goddard Earth Sciences Technology and Research, Universities Space Research Association, Columbia, Maryland, USA.

<sup>2</sup>NASA Goddard Space Flight Center, Greenbelt, Maryland, USA.

<sup>3</sup>Department of Earth and Planetary Science, Johns Hopkins University, Baltimore, Maryland, USA.

<sup>4</sup>Computational Physics Inc., Springfield, Virginia, USA.

<sup>5</sup>Science Systems and Application Inc., Lanham, Maryland, USA.

Corresponding author: F. Li, NASA Goddard Space Flight Center, Code 614, Greenbelt, MD 20771, USA. (feng.li@nasa.gov)

©2012. American Geophysical Union. All Rights Reserved.  
0148-0227/12/2012JD017905

[4] A major concern of the model results is that the mechanism for the decrease of the mean age is not clear. Previous studies have shown that the increase of the residual circulation plays an important role in driving the trend of the mean age [Austin and Li, 2006; Garcia et al., 2007; Oman et al., 2009], but there is not a complete understanding how these two processes are related. Strahan et al. [2009] demonstrated that in the tropical pipe the timescale of the residual circulation is significantly smaller than the mean age. The differences between the two timescales are caused by recirculation of air parcels between the tropics and mid-latitudes. An air parcel could make multiple transits between the tropics and midlatitudes. This recirculation process depends on mixing through the subtropical transport barriers [Neu and Plumb, 1999]. Thus changes in recirculation and mixing also impact the trend of the mean age. But it is not clear how recirculation and mixing respond to greenhouse gas increases and how these responses impact the mean age.

[5] Investigating long-term age spectrum changes helps to clarify the roles of changes in the residual circulation, recirculation and mixing in driving the decrease of the mean age. The age spectrum is the probability distribution function of transit times between a source region in the troposphere or at the tropopause and a sample region in the stratosphere [Hall and Plumb, 1994; Waugh and Hall, 2002]. The mean age is the first moment of the age spectrum, or an average of all the possible transit times. In addition to the mean age, other important parameters that characterize the age spectrum include the modal age and spectral width. The modal age corresponds to the time of the spectral peak. It represents the most probable transit time and is directly associated with the timescale of the bulk velocity of tracer transport [Waugh and Hall, 2002]. The modal age agrees very well with the timescale of the residual vertical velocity within the tropical pipe region [Strahan et al., 2009]. The spectral width is related to the second moment of the age spectrum and is a measure of the recirculation strength [Strahan et al., 2009]. The age spectrum contains complete information on transit times and is more useful than the mean age in understanding the distribution of photochemically important trace species in the stratosphere [Schoeberl et al., 2005; Waugh et al., 2007]. While the decrease of the mean age in the 21st century model simulations has been extensively documented, no previous studies have investigated the long-term changes in the age spectrum.

[6] In this paper we investigate the long-term changes in the stratospheric age spectra in the 21st century using a simulation with the Goddard Earth Observing System Chemistry-Climate Model (GEOSCCM). The main purposes of this study are to characterize the long-term changes in the age spectra and to identify processes that cause the decrease of the mean age. This paper is organized as follows. A brief review of the age spectrum theory and a detailed description of our method to calculate the age spectrum are given in section 2. This is followed by an introduction of the GEOSCCM and the experiment setup in section 3. Results and discussion are presented in section 4. Conclusions are given in section 5.

## 2. Method

[7] The age spectrum is a Green's function, or a boundary propagator, that solves the continuity equation for the

mixing ratio of a conserved and passive tracer [Hall and Plumb, 1994]. It is also called the Transit-Time Distribution (TTD) in the ocean and tropospheric transport literature [Holzer et al., 2003; Haine et al., 2008]. The age spectrum is expressed by

$$\chi(r, t) = \int_0^{\infty} \chi(\Omega, t - \xi) G(r, t | \Omega, t - \xi) d\xi. \quad (1)$$

[8] Here  $\chi(r, t)$  is the tracer mixing ratio at a sample region  $r$  and sample time  $t$ ,  $\xi$  is the elapsed time between the sample time  $t$  and source time  $t'$  (i.e.,  $\xi = t - t'$ ), the source time  $t'$  is when the tracer had last contact with the boundary source region  $\Omega$ ,  $\chi(\Omega, t - \xi)$  is the source time history at the boundary source region, and  $G(r, t | \Omega, t - \xi)$  is the age spectrum. The physical meaning of the age spectrum is clear in equation (1):  $G(r, t | \Omega, t - \xi) d\xi$  represents the mass fraction of the air parcel at  $r$  and  $t$  that was last in contact with  $\Omega$  between  $\xi$  and  $\xi + d\xi$  ago.

[9] Different methods have been used to calculate age spectra [e.g., Hall and Plumb, 1994; Schoeberl et al., 2003; Haine et al., 2008]. Among all the methods that have been used, the pulse tracer method is the most direct approach. It should be emphasized that the pulse tracer method does not directly produce age spectra. Instead it generates another kind of boundary propagator  $G(r, t' + \xi | \Omega, t')$ , which is called the Boundary Impulse Response (BIR) [Haine et al., 2008; Li et al., 2012]. Once BIRs are obtained, they can be used to calculate age spectra.

[10] Replace  $t$  with  $t' + \xi$ , then equation (1) becomes

$$\chi(r, t' + \xi) = \int_0^{\infty} \chi(\Omega, t') G(r, t' + \xi | \Omega, t') d\xi. \quad (2)$$

[11] Note that if we set the boundary condition of  $\chi(\Omega, t')$  as a Dirac delta function, then equation (2) yields  $\chi(r, t' + \xi) = G(r, t' + \xi | \Omega, t')$ . Thus the BIR is the time evolving response to a delta function boundary condition. The BIR can be easily calculated in models using the pulse tracer: release a pulse of a conserved and passive tracer at a chosen source region and source time, and the time series of the tracer's mixing ratio at any interior point  $r$  is  $G(r, t' + \xi | \Omega, t')$ .

[12] The mathematic relationship between the BIR and the age spectrum is simple, but equation (2) does not have the same clear physical meaning as equation (1). It is important to recognize that the age spectrum and the BIR are different due to their time dependence. Only in the special case of steady flow is the age spectrum the same as the BIR. Computing the age spectrum in unsteady flow is more complicated and requires a series of BIRs that are launched at different source times [Holzer et al., 2003; Haine et al., 2008; Li et al., 2012]. There are two approaches. If one is interested in the seasonal and interannual variability of the age spectra, then one needs to reconstruct time varying age spectra from BIRs [Li et al., 2012]. But if one is mainly interested in the time-averaged properties of the age spectra, one can use the mean of an ensemble of BIRs as a time-averaged age spectrum. This is because the BIR and the age spectrum share the same boundary propagator distribution [Haine et al., 2008].

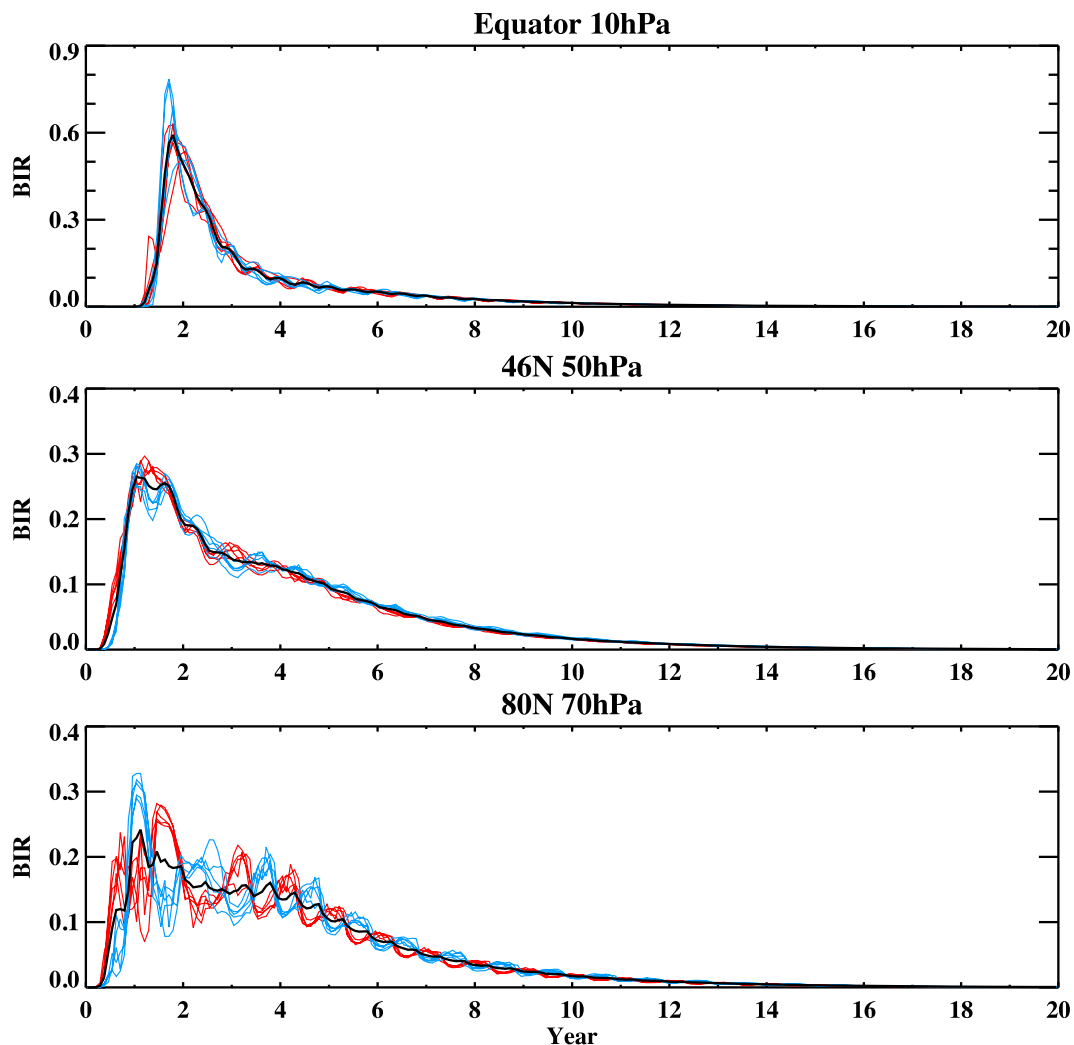


**Figure 1.** Examples of the Boundary Impulse Responses (BIRs) in 2000–2019 at three locations. For this 20-year period, five BIRs are released in January (red) and five BIRs are released in July (blue) of 2000–2004. The thick black line is the age spectrum, which is calculated as the mean of the ten BIRs. The unit is 1/month.

[13] The stratospheric transport has large seasonal and interannual variations. This variability has to be accounted for in order to correctly capture the annual mean or the seasonal properties of the age spectra. *Li et al.* [2012] investigated the seasonal variations of the stratospheric age spectra in the GEOSCCM. They reconstructed seasonally varying age spectra from twelve BIRs released in each month of the annual cycle. Here, we focus on the long-term changes in the time-averaged properties of the age spectra, and take the second approach introduced above to use the mean of an ensemble of BIRs launched in different times as the time-averaged age spectra.

[14] The method of *Hall et al.* [1999a] is followed to conduct the pulse tracer experiment. The tropical lower troposphere between 10 N and 10 S and from the surface to about 800 hPa is chosen to be the boundary source region. As an approximation of a delta function boundary condition, the tracer is set to an arbitrary positive value in the first month of the experiment and then held as zero through the rest of the experiment in the boundary source region. There are no

other sources or sinks for the tracer. The pulse experiment runs for 20 years.

[15] We perform a 21st century (2000 to 2100) transient simulation with the GEOSCCM using time-varying  $\text{CO}_2$  from scenario A1b [*Intergovernmental Panel on Climate Change (IPCC)*, 2001] with other greenhouse gases and chlorofluorocarbons (CFCs) fixed to the year 2000 levels [*World Meteorological Organization*, 2007]. We release pulses in January and July of the first five years in the periods: 2000–2019, 2020–2039, 2040–2059, 2060–2079, and 2080–2099. Hence, each of these 20-year periods includes 10 pulses. The different release times of the pulse tracers are chosen to represent the seasonal and interannual variability of stratospheric transport. BIRs are calculated for each of these 20-year periods, for a total of fifty BIRs, with age spectra calculated for the model years 2000–2019, 2020–2039, 2040–2059, 2060–2079, and 2080–2099.

[16] Figure 1 shows examples of the BIRs and their ensemble mean in 3 different locations in the 2000–2019 period. The BIRs released in January and July are shown in

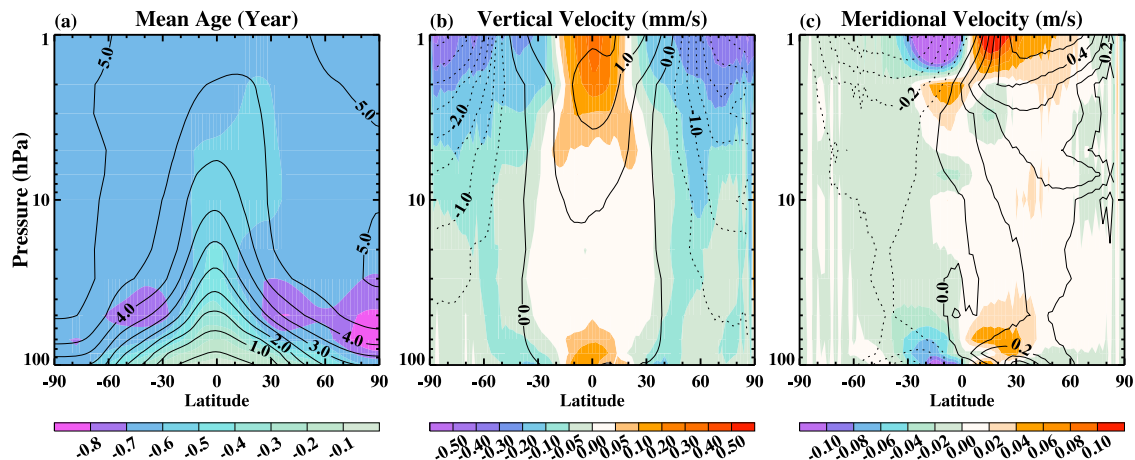


**Figure 2.** (a) Distribution of the 2000 age spectrum mean age (contours) and the differences in the mean age between the 2080 and 2000 age spectra (color). (b) Distribution of the residual vertical velocity for the period 2000–2019 (contours) and the differences in the residual vertical velocity between 2080–2099 and 2000–2019 (color). (c) Same as Figure 2b, but for the residual meridional velocity.

red and blue, respectively. The BIRs have strong seasonal and interannual variability. In the tropics, the interannual variability reflects the impacts of the quasi-biennial oscillation (QBO) on the BIRs. In the extratropics, seasonal differences of the BIRs stand out, although there are considerable interannual variations. The age spectrum (thick black line), i.e., the ensemble mean of the BIRs, is different from the ensemble members. Therefore it is important to use an ensemble of BIRs in order to accurately capture the time-averaged properties of the age spectra.

### 3. GEOSCCM and Simulation

[17] The model we use in this study, the GEOSCCM [Pawson *et al.*, 2008], couples the GEOS5-AGCM [Rienecker *et al.*, 2008] with a comprehensive stratospheric chemistry package [Douglass *et al.*, 1997]. The GEOSCCM has 72 vertical levels with a model top at 0.01 hPa. The horizontal resolution in the GEOSCCM is adjustable and a grid of  $2^\circ$  latitude by  $2.5^\circ$  longitude is used in this study. The pulse tracer experiments were carried out with a sensitivity simulation of the 21st century in which  $\text{CO}_2$  increases under the IPCC [2001] A1b scenario, but the amount of ozone depleting substances (ODSs) and other greenhouse gases are fixed at the year 2000 level conditions. The simulation uses modeled sea surface temperature and sea ice in the 21st century under the A1b scenario from the NCAR Community Climate System Model 3.0. In this sensitivity simulation, the model climate change is solely driven by increases in  $\text{CO}_2$  and sea surface temperature. As described in detail in the previous section, a total of fifty pulse tracer experiments are carried out with the simulation. Fifty BIRs are generated and five age spectra are computed. In the rest of the paper, the five age spectra are referred as 2000, 2020, 2040, 2060, and 2080 spectra, respectively. All results presented in this paper are zonally and monthly averaged.

[18] The GEOSCCM was evaluated in the Chemistry-Climate Model Validation Activity 2 (CCMVal-2) and was found to have a realistic representation of stratospheric chemistry, transport, and dynamics [SPARC CCMVal, 2010;

Strahan *et al.*, 2011]. The GEOSCCM demonstrates realistic stratospheric transport characteristics, such as the mean age, the tropical ascent rate, and the lower stratospheric mixing rate. However, the Antarctic polar vortex is more isolated in the GEOSCCM than observed, a common bias in CCMs. The version of the GEOSCCM used in this study is slightly different from the one evaluated in CCMVal-2 in that it includes a QBO that is produced by increasing non-orographic gravity wave sources in the tropics.

## 4. Results and Discussion

### 4.1. Long-Term Changes in Age Spectra

[19] Our simulation projects a decrease in the mean age of air and an increase in the residual circulation in the 21st century, consistent with previous CCM studies [e.g., Butchart *et al.*, 2006, 2010]. Figure 2a shows the differences in the mean age between the 2080 and 2000 spectra, where the mean age is computed from the age spectrum by

$$\Gamma(r, t) = \int_0^\infty \xi G(r, t | \Omega, t - \xi) d\xi. \quad \text{The mean age is younger}$$

in 2080 than in 2000 everywhere in the stratosphere. The rate of decrease is larger in the midlatitudes than in the tropics, indicating a reduced mean age gradient between these two regions and an enhanced tropical ascent rate [Neu and Plumb, 1999]. A strong decrease in the mean age is found in the subtropical and midlatitude lower stratosphere in both hemispheres, suggesting an increase of the quasi-horizontal transport in this region. In the northern hemisphere lower stratosphere the area of large mean age decrease extends to the polar region. The largest decrease in the mean age is found in the Arctic lower stratosphere (over 0.8 years, or 20%). This suggests the acceleration of the quasi-horizontal transport is particularly strong in the northern hemisphere. Overall these results agree well with those produced by the version of the GEOSCCM evaluated in CCMVal-2 [Butchart *et al.*, 2010], although the decrease of the mean age is larger in the current simulation. Note that in the CCMVal-2

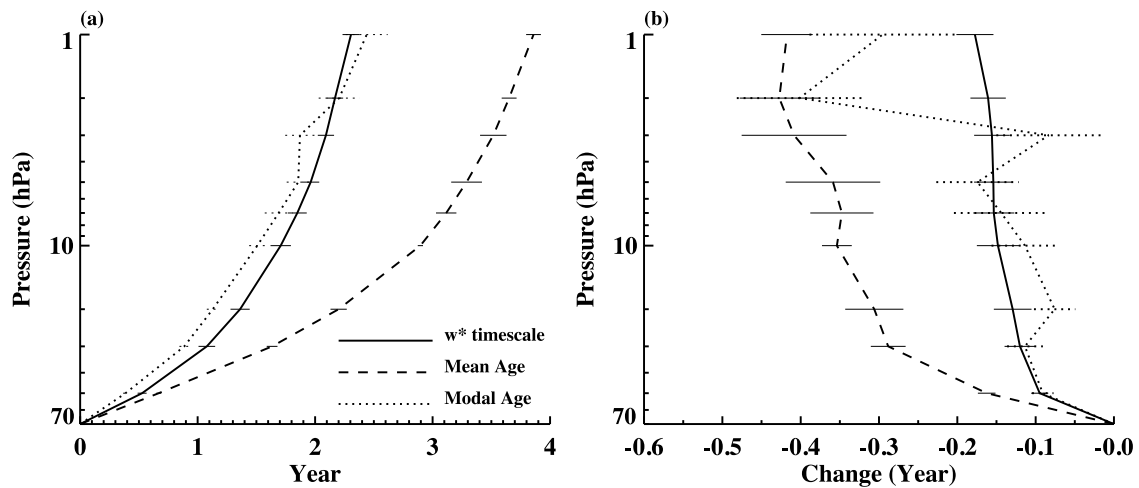


**Figure 3.** (a) Comparison of the mean age (dashed), modal age (dotted), and the timescale of the residual vertical velocity in the tropical pipe region (10 S – 10 N, 70 hPa – 1 hPa) in the period 2000–2019. The error bars represent interannual variations of these three timescales. (b) Difference in the mean age (dashed), modal age (dotted) and the timescale of the residual velocity in the tropical pipe region between 2080–2099 and 2000–2019.

simulation the GEOSCCM simulated ozone recovery in the 21st century, while the simulation considered here has fixed CFCs. A larger decrease in the mean age without ozone recovery is consistent with the findings of *Oman et al.* [2009] that ozone recovery in the 21st century acts to reduce the rate of mean age decrease. The stronger tropical non-orographic gravity wave drag in this simulation may also contribute to the larger mean age decrease.

[20] The decrease in the mean age of air is consistent with the acceleration of the residual circulation (Figures 2b and 2c). Changes in the residual vertical velocity ( $\bar{w}$ ) and meridional velocity ( $\bar{v}$ ) clearly show cells in each hemisphere. The increase in the residual velocities is much stronger in the lower and upper stratosphere than in the middle stratosphere. Within each cell, the increase in the tropical upwelling is balanced by an increase in the poleward mass transport and an increase of extratropical downwelling. Changes in the lower branch of the residual circulation are confined to the tropics and mid-latitudes, whereas the increase of the upper stratospheric residual circulation extends all the way to the high latitudes.

[21] Previous studies have shown that the mean age is strongly correlated with the tropical upward mass flux in the lower stratosphere, a measure of the overall strength of the residual circulation [Austin and Li, 2006; Butchart et al., 2010]. But the timescale of the residual circulation should not be confused with the mean age. The residual velocity approximates the bulk velocity of tracer transport. *Waugh and Hall* [2002] showed that the timescale of the residual circulation (or bulk tracer transport) is closely associated with the modal age in regions of weak mixing such as the tropical pipe. The modal age and the timescale of the residual circulation are smaller than the mean age because the stratospheric age spectrum has a skewed distribution with a long tail [Hall and Plumb, 1994]. *Schoeberl et al.* [2008] calculated the vertical velocity for water vapor advection from the tape recorder signal in the tropical pipe and found that it agrees very well with the residual vertical velocity. *Strahan et al.* [2009] further showed that the modal age is a lower limit of

the timescale of the residual vertical velocity and both are shorter than the mean age.

[22] In order to illustrate the relationship between the mean age, the modal age, and the timescale of the residual circulation, Figure 3 shows a vertical plot (70–1 hPa) of these three timescales in the tropical pipe region (10 S–10 N). First we note that the transit time of the mean vertical advection is closely associated with the modal age and is significantly shorter than the mean age, confirming the results of *Strahan et al.* [2009]. Mean age, modal age, and the vertical advection timescale all decrease between 2080–2099 and 2000–2019 (Figure 3b). These decreases in the vertical advection timescale and modal age are comparable to each other in most of the stratosphere, and they are distinctly smaller than the decrease of the mean age. In terms of the absolute value, decreases in the mean age are more than twice those in the transit time of the vertical advection. The relative changes in the mean age are also larger than that in the transit time of the vertical advection (not shown). This example shows that the decrease of the mean age is only partly explained by the acceleration of the residual circulation.

[23] Figure 4 shows the distributions of the modal age (a) and spectral width (b) of the 2000 spectra (contours) and the differences between the 2080 and 2000 spectra (color). The distribution of the modal age is somewhat similar to the mean age, but the modal age has stronger gradients in the high latitude lower stratosphere. The modal age increases 2–4 times in a very narrow latitudinal band in this region. From 2000 to 2080 the modal age decreases in most of the stratosphere. The changes in the modal age are less smoothly distributed than the changes in the mean age. In general the decrease in the modal age in terms of absolute value is smaller in the tropics than in the high latitudes. The largest decrease is seen in the polar lower stratosphere, especially in the Arctic. We will show later that the large change of the modal age in the polar lower stratosphere is caused by change in the multimodal spectral shape in this region.

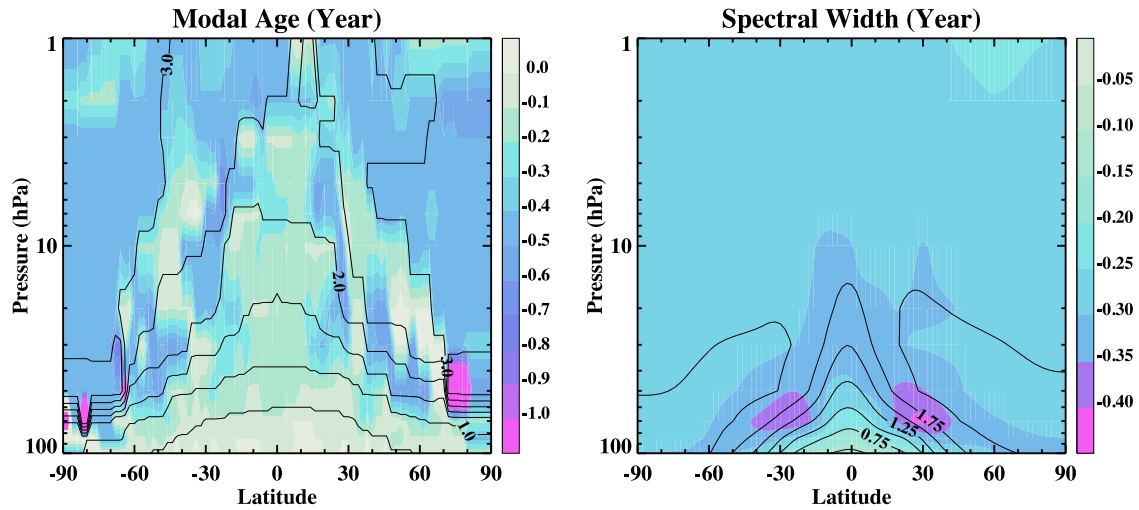


**Figure 4.** The color shadings are differences in the (left) modal age and (right) spectral width between the 2080 and 2000 age spectra. The contours are the (left) modal age and (right) spectra width of the 2000 age spectra.

[24] The spectral width is related to the square root of the second moment of the age spectrum by  $\Delta(r, t) =$

$$\sqrt{\frac{1}{2} \int_0^{\infty} (\xi - \Gamma(r, t))^2 G(r, t | \Omega, t - \xi) d\xi}.$$

It quantifies the spread of the transit time distribution [Waugh and Hall, 2002]. Qualitatively, the width indicates how the spectrum tail contributes to the mean age. A greater width implies a longer tail, and thereby a greater fractional contribution by the tail to the mean age. The tail of the age spectrum is related to the strength of the recirculation, thus the width can also be viewed as a measure of the strength of the recirculation [Strahan et al., 2009]. Figure 4b shows that the distribution of the spectral width is similar to that in the mean age below about 10 hPa (compare to Figure 2a), but the width becomes uniform with a value of about 2 years above 10 hPa. Throughout the stratosphere, the spectral width decreases from 2000 to 2080. The largest decreases in the width are found in the subtropical (20–40° N and S) lower stratosphere.

[25] We now examine the distribution of the age spectra and their changes at 50 and 10 hPa. Our focus is on the lower stratosphere because the largest changes in the mean age, modal age, and spectral width occur below 10 hPa. Figure 5 shows the 2000 age spectra at 50 hPa and the differences between the 2080 and 2000 age spectra as a function of latitude. The age spectra have skewed distributions with young peaks and long tails. Only the first 10 years of the age spectra are shown because the tail of the spectra decays rapidly with increasing transit time. The age spectra have large latitudinal variations with younger and stronger peaks and more compact distributions in the tropics than in the extratropics. The modal age (dotted line) has very sharp gradients around 70° latitude in both hemispheres with values increasing by more than 2 times in a narrow latitudinal band.

[26] The 2080 age spectra have higher percentages of young air and lower percentages of old air compared to the 2000 age spectra (Figure 5b). The transition from positive (more young air, warm color) to negative (less old air, cold color) 2080–2000 differences follows approximately the modal age of the 2000 age spectra (black dotted line). This indicates that the spectral peaks become younger and stronger in the 2080 spectra. These changes lead to decreases in the mean age and spectral width. Furthermore, younger and stronger spectral peaks together with narrower widths mean that the 2080 age spectra have shorter tails. There are multiple peaks at high latitudes, suggesting the age spectra in this region have a multimodal shape [Li et al., 2012].

[27] Overall the 10 hPa age spectra are similar to the 50 hPa age spectra, although they have smaller latitudinal variations, especially in the spectral width (Figure 6a). The changes between the 2080 and 2000 age spectra at 10 hPa are also similar to those at 50 hPa (Figure 6b). Again the 2080 spectra have a larger fraction of young air than the 2000 age spectra and the change from more young air to less old air occurs at about the time of the modal age of the 2000 spectra. A notable difference is that the 10 hPa 2080–2000 differences at high latitudes do not show multiple peaks.

[28] We investigate the changes in age spectra in the lower stratosphere in more detail by examining the evolution of the age spectra at 50 hPa in different locations. Figure 7 clearly shows that as the integration progresses, the modal ages become younger, the spectral peaks get stronger, the tails are shorter, and the widths are narrower. The age spectra undergo larger changes between 2020–2039 and 2040–2059 than in other periods.

[29] The 50 hPa age spectra at high latitudes have different characteristics from those at low and middle latitudes. They have multiple peaks, in contrast to the single-modal shape at lower latitudes. For example, in the Arctic the 2000 spectrum (black line) has 3 peaks between 3 and 4 years of transit time (Figure 7e). The strongest peak, which is just slightly

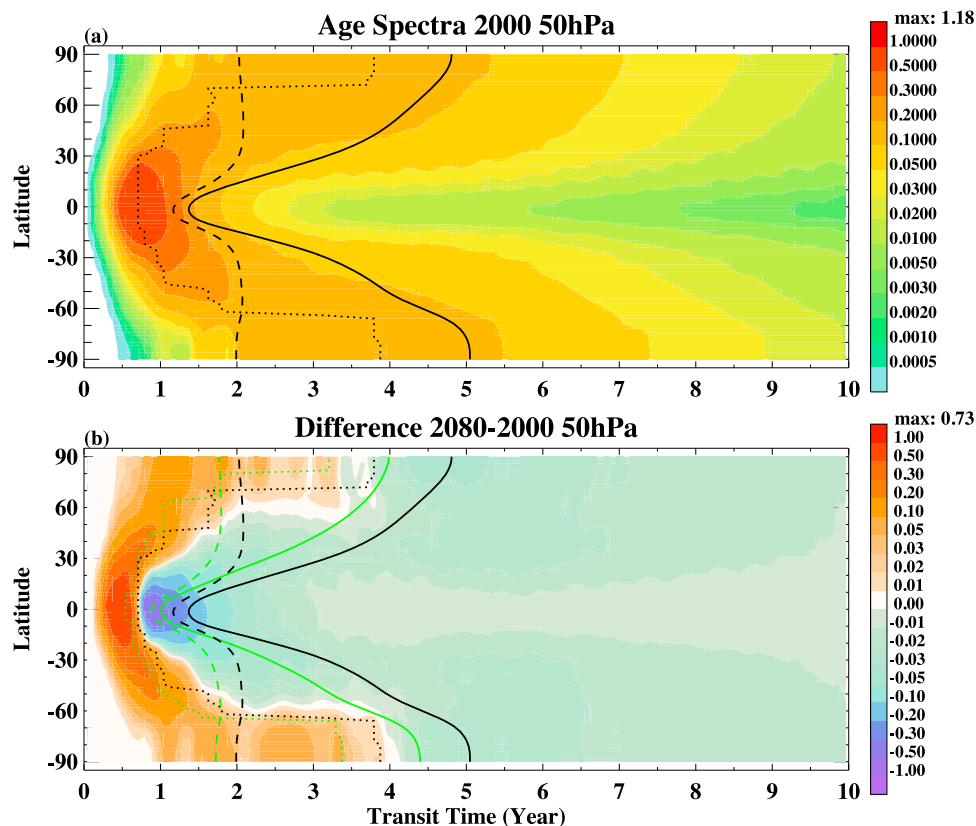


**Figure 5.** (a) Distribution of the 2000 age spectra at 50 hPa as a function of latitude. The black solid, dashed, and dotted lines are the mean age, spectral width, and modal age, respectively. (b) Differences between the 2080 and 2000 age spectra at 50 hPa. The black lines are the same as in Figure 5a. The green solid, dashed, and dotted lines are the mean age, spectral width, and modal age in the 2080 age spectra, respectively. In both panels the color scales are normalized to the maximum value shown at the top of the color bar. The unit is 1/month.

stronger than other peaks, occurs at 3.7 years. In the 2080 spectrum (red line in Figure 7e) the peak at 1.8 years becomes the strongest among several comparable peaks, and we obtain a decrease of modal age of 1.9 years from 2000 to 2080. The dramatic modal age change in the polar stratosphere (also see Figure 4a) reflects the changes of relative strength of the multiple peaks.

[30] The change from a single-modal shape in the low and middle latitudes to a multimodal shape in the high latitudes has been reported previously [Reithmeier *et al.*, 2008; Li *et al.*, 2012]. However, these studies showed that the multiple peaks in the polar age spectra have an annual cycle, whereas here these peaks have a semi-annual cycle (Figures 7e and 7f). Examining Figure 1 (especially Figure 1 (bottom)) reveals that this semi-annual cycle is caused by the semi-annual phase difference of the January and July BIRs. This bias can be improved by releasing more pulse tracers per year to represent the full seasonal cycle of the BIRs and hence to better capture the time-mean properties of the age spectrum.

#### 4.2. Decrease of the Age Spectrum Tail

[31] The results presented in Figures 5–7 indicate that the decrease of the mean age in the 2080 age spectra is due to an

increase in the percentages of the young air and a decrease in the percentages of the old air, or the tail of the age spectra. Changes in the tail of the age spectra can be more easily seen when the age spectra are plotted in the logarithmic scale. Figure 8 is the same as Figure 7, but it uses the logarithmic scale and covers the whole 20-year period. There are several interesting features regarding the distribution and changes of the tail. First, the logarithm of the spectrum tail can be represented by a straight line. That is, the tail is very well approximated by an exponential decay function  $\Psi_0(r, t) \exp\left(-\frac{t}{\tau_0}\right)$ , where  $\tau_0$  is the decay timescale. Second, the slope of the tail, or the decay timescale  $\tau_0$ , appears to be independent of locations. Third, the tails are shorter in 2080 than in 2000. The decrease in the tail can be quantified by a decrease in  $\tau_0$ .

[32] The decay timescale  $\tau_0$  has long been known as a fundamental stratospheric transport diagnostic [Prather 1996; Hall *et al.*, 1999b; Ehhalt *et al.*, 2004]. Under the steady state condition, the age spectrum can be decomposed into a set of normal modes, each of which decays exponentially at a timescale that is equal to the inverse of its eigenvalue [Hall *et al.*, 1999b]. The base mode has the longest decay timescale  $\tau_0$  and it decays more slowly than the higher

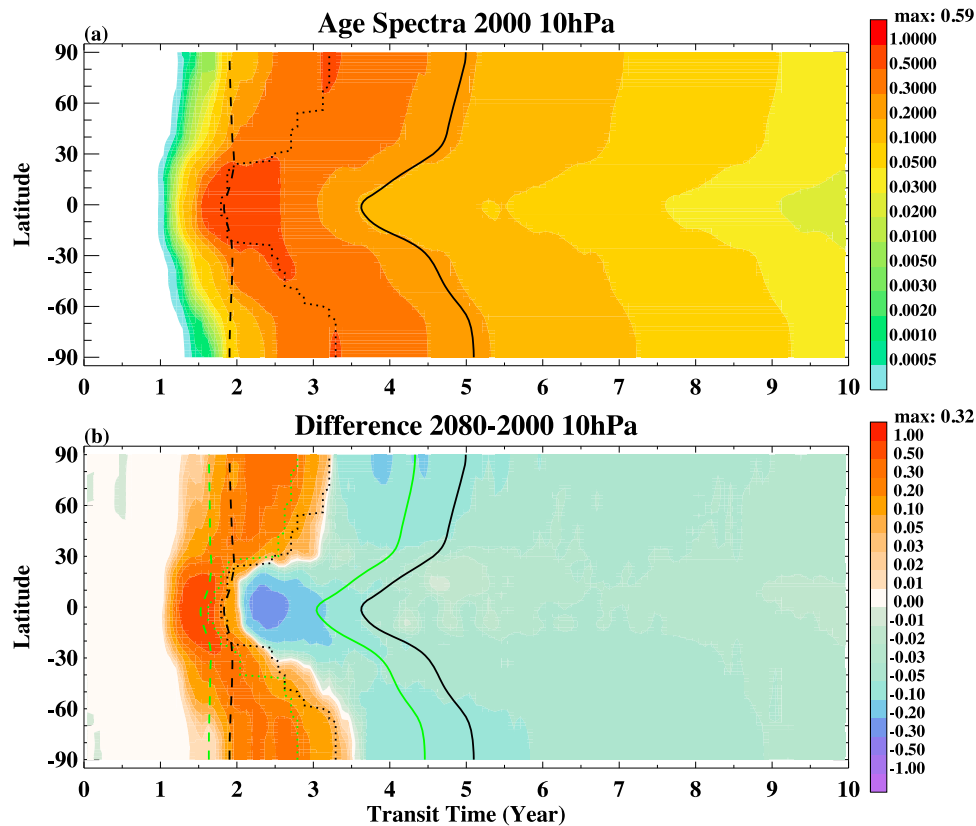


**Figure 6.** Same as Figure 5, but for age spectra at 10 hPa.

modes. For long transit time, only the base mode survives and thus the tail of the age spectrum can be approximated by the base mode.  $\tau_o$  is a unique transport diagnostic because it is independent of location. Physically  $\tau_o$  describes how fast the mixing ratio of a conserved tracer in the stratosphere decays due to transport alone [Ehhalt *et al.*, 2004]. It can also be viewed as an integrated measure of the strength of stratospheric recirculation.

[33] The decrease in the mean age of air through the 21st century is strongly correlated with the decrease of  $\tau_o$ . Figure 9a plots the evolution of  $\tau_o$  from 2000 to 2080 against the globally and stratospherically (100–1 hPa) averaged mean age. When calculating  $\tau_o$ , the tail of the age spectra is regressed onto a single exponential decay mode. Here we define the tail as the region with transit time older than 4 years, noting that the age spectra start to exponentially decay at about 4 years (see Figure 8). The correlation between  $\tau_o$  and the mean age is 0.998, though we only have 5 samples. This strong correlation indicates that the decrease of the mean age is closely related to the decrease of the tail of the age spectra.

[34] The decrease of  $\tau_o$  is highly anti-correlated with the increase of the upward mass flux in the tropical lower stratosphere (Figure 9b), which means that an accelerated residual circulation acts to weaken the stratospheric recirculation. It is known that changes in mixing across transport barriers could affect recirculation [Neu and Plumb, 1999; Strahan *et al.*, 2009], but our results show that the

stratospheric mean meridional circulation has a significant impact on recirculation and the tail part of the age spectra (also see discussion in Section 4.3). It remains to be determined whether the real atmosphere would respond to an accelerated residual circulation in the same way as simulated by our model.

[35] The age spectrum tail has received less attention than other spectral parameters in previous studies, but the tail has a significant impact on the mean age [Schoeberl *et al.*, 2003, 2005]. Mean age can be regarded as the mixing ratio of an ideal clock tracer that has a linearly increasing stratospheric source and a fixed tropospheric concentration [Vaugh and Hall, 2002]. Therefore the spectrum tail weighs heavily on the mean age. Figure 10a shows the fractional contribution of the tail (solid contours, defined as transit times older than 4 years) to the mean age in the 2000 spectra and the changes of the fractional contribution between the 2080 and 2000 spectra (color). The pattern of the contribution by the tail looks similar to the mean age (Figure 2a). The tail contributes a smaller fraction to the mean age in the tropical lower stratosphere where the age spectra are dominated by young spectral peaks. In the rest of the stratosphere, however, the tail accounts for more than 50% of the mean age. From 2000 to 2080, the tail becomes shorter and its fractional contributions to the mean age decrease everywhere in the stratosphere. The largest decrease of the tail contribution occurs in the subtropical lower stratosphere between 20° and 30° latitudes and centered at 70 hPa, which corresponds to

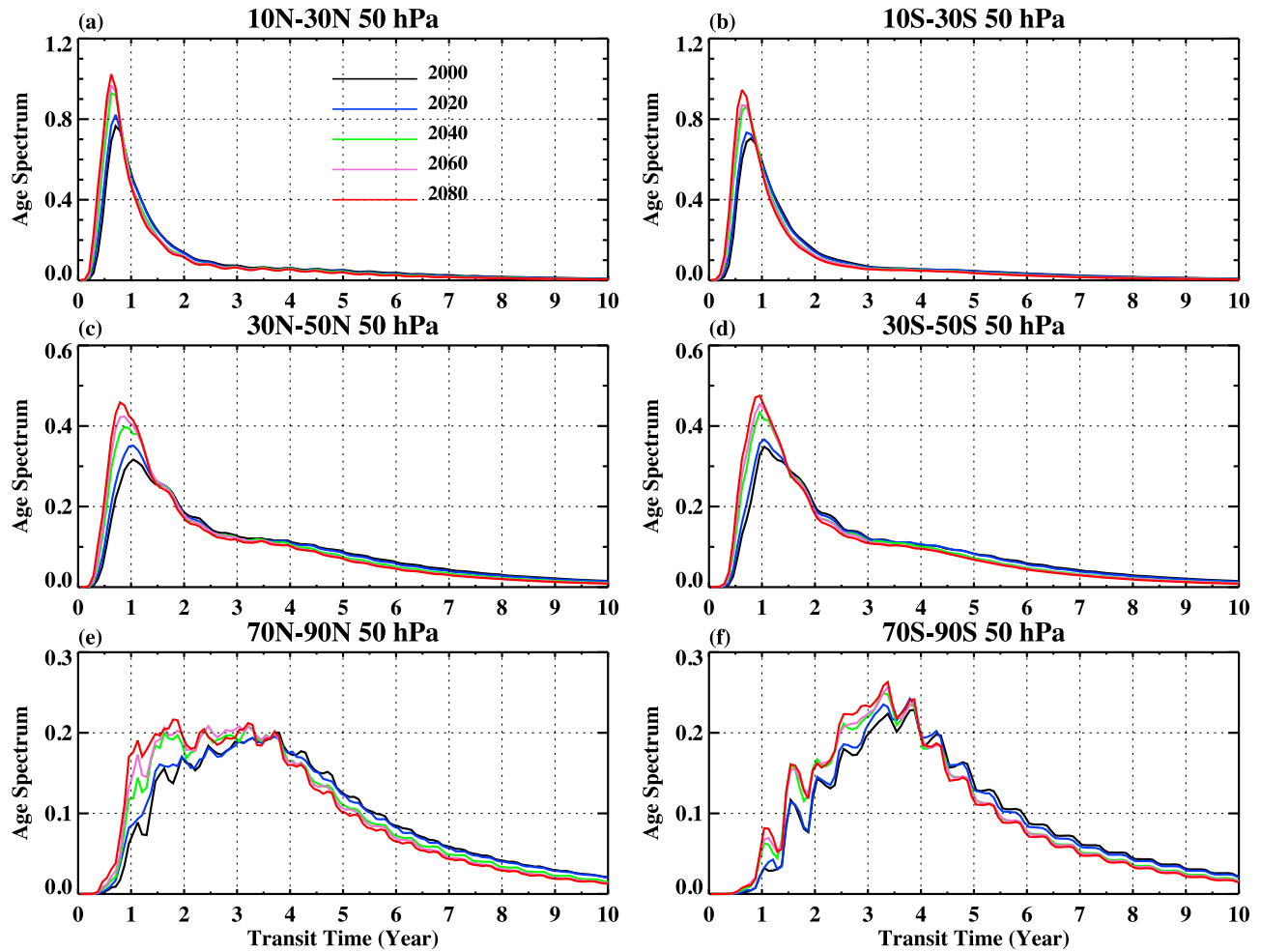


**Figure 7.** Evolution of the age spectra in the 21st century at different locations at 50 hPa.

the largest decrease in the spectral width (see Figure 4b). This correspondence is expected since the width is closely linked with the tail. The changes in the tail can also be quantified by the changes in the averaged transit time in the

$$\text{tail } \Gamma_{\text{tail}} = \int_{4 \text{ year}}^{20 \text{ year}} \xi G d\xi, \text{ referred to as the tail age here.}$$

Comparing Figure 10b with Figure 2a (color) reveals that the tail age decreases more than the mean age between 2080 and 2000. This confirms that the decrease in the tail indeed makes an important contribution to the decrease in the mean age.

### 4.3. Long-Term Changes in Isentropic Mixing

[36] In addition to the residual circulation, changes in isentropic mixing could also impact the trend of the mean age and age spectra. For instance, enhanced mixing from the midlatitudes to the tropics increases the probability of recirculation within the stratosphere, and thus leads to a longer tail, a wider width, and an older mean age [Neu and Plumb, 1999; Strahan *et al.*, 2009]. However, it is not clear how stratospheric mixing might change in the 21st century, and

what the impacts the changes in mixing would have on the age spectra. Here we calculate the equivalent length of  $\text{N}_2\text{O}$  to investigate the long-term changes in isentropic mixing. The equivalent length of a chemical tracer measures the geometry complexity of the tracer contours in the equivalent latitude coordinate on isentropic surfaces [Nakamura, 1996; Ma *et al.*, 2003]. Nakamura [1996] showed that the equivalent length, or more accurately its square, is a useful diagnostic of the efficiency of isentropic tracer mixing.

[37] Figure 11 shows the distribution of the normalized equivalent length squared of  $\text{N}_2\text{O}$  ( $\eta$ ) for 2000–2019 (contours) and the relative differences between 2080–2099 and 2000–2019 (color). Large values of  $\eta$  correspond to strong mixing, whereas small values indicate weak mixing, or transport barrier. For example, the surf zone can be recognized by large values of  $\eta$  in the midlatitudes, while the subtropical and polar vortex barriers can be identified respectively by small values of  $\eta$  in the subtropics and polar region. The base of the tropical pipe, identified by strong gradient in  $\eta$  in the tropical lower stratosphere, has a “V” shape. Large values of  $\eta$  are also found in the tropical/subtropical lower stratosphere, corresponding to the so-called “tropically controlled transition region.” In order to test the

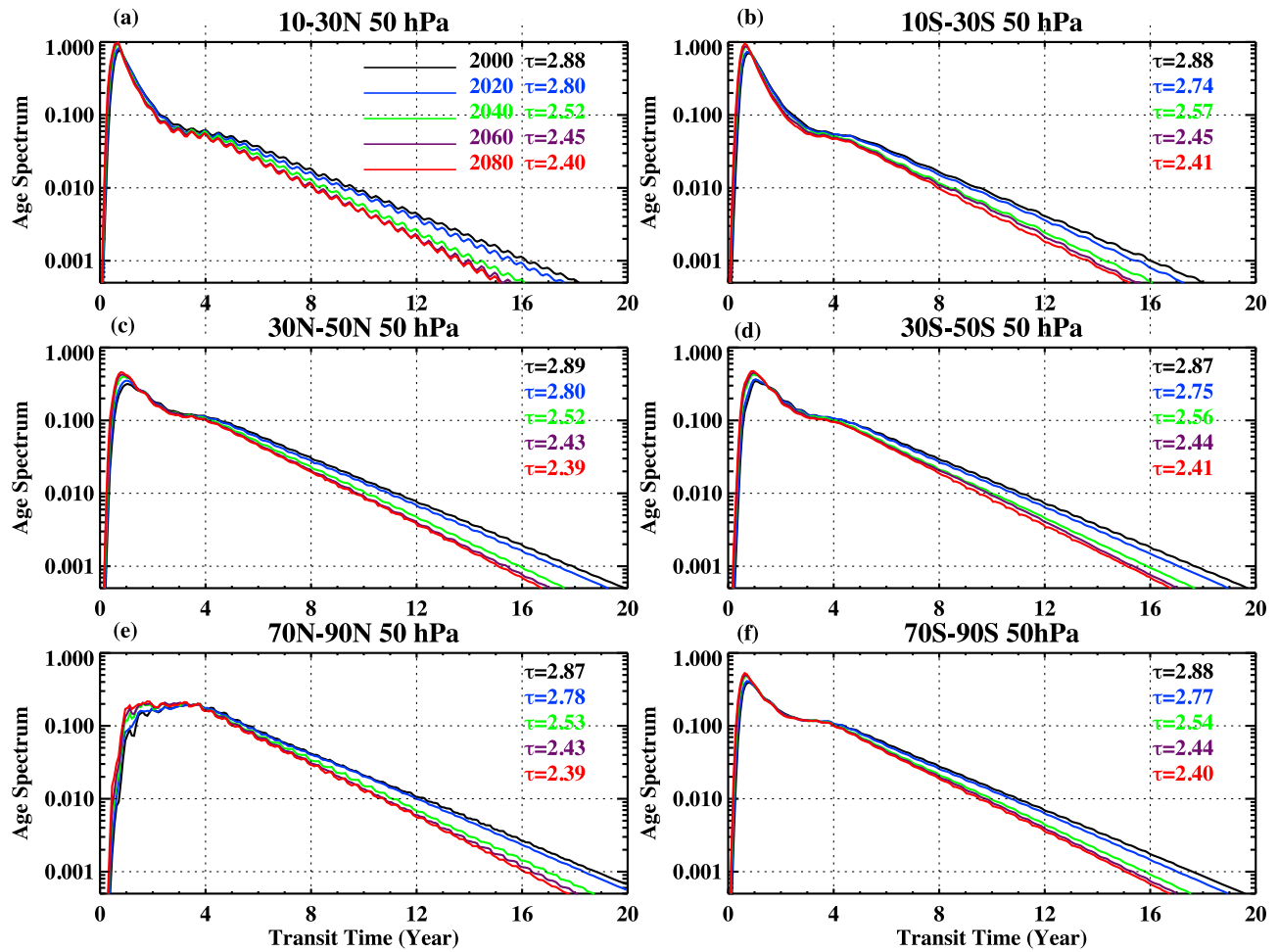


Figure 8. Same as Figure 7, but on logarithmic scale.

robustness of these results, we also calculate the equivalent length using  $\text{CH}_4$  and find almost exactly the same results (not shown). This gives us confidence in using the equivalent length to diagnose changes in stratospheric mixing.

[38] The most striking feature in the changes of  $\eta$  between 2080–2099 and 2000–2019 is a large increase in  $\eta$  in the tropical/subtropical lower stratosphere. Mixing increases up to 50% in the base of the tropical pipe. There are essentially

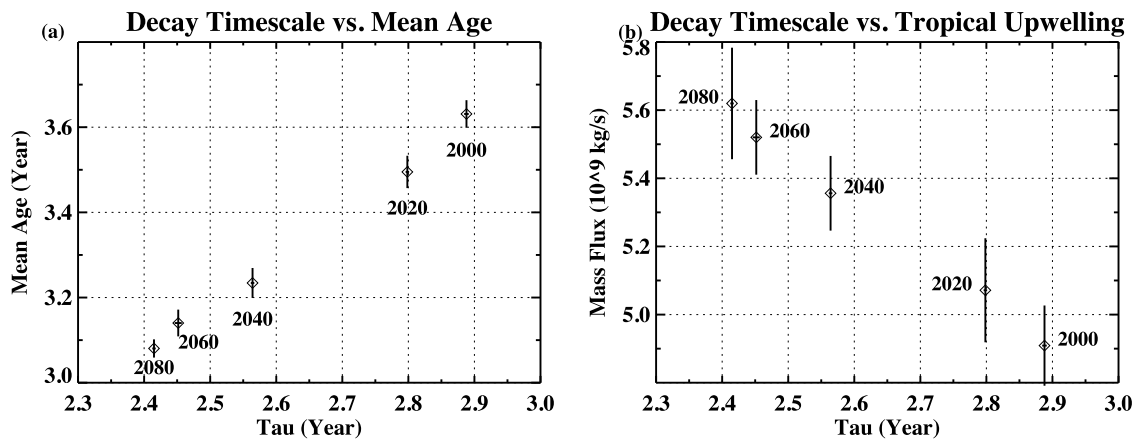
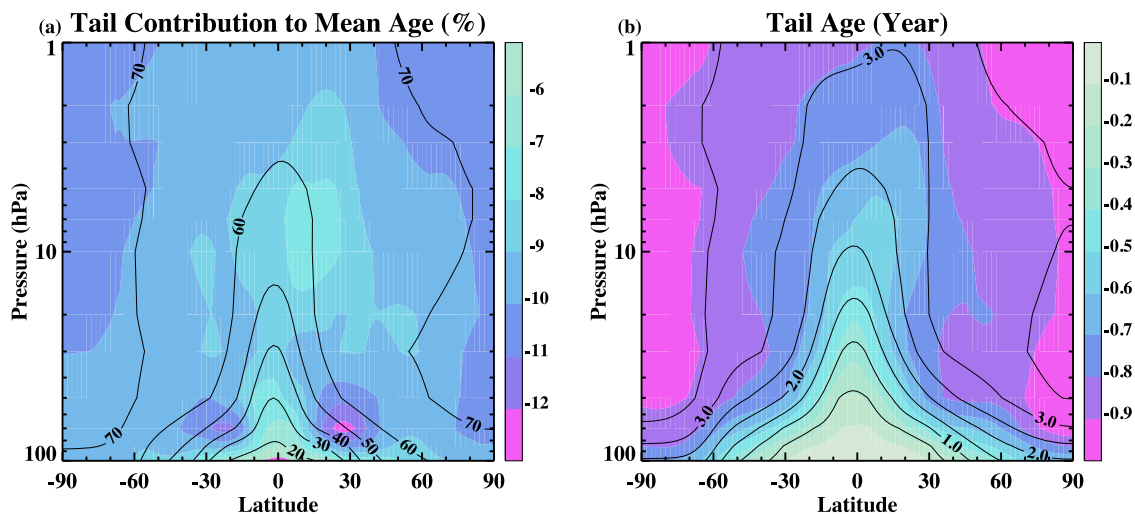


Figure 9. (a) The scatterplot of the decay timescale of the tail of the age spectra against the globally and stratospherically averaged (100 – 1 hPa) mean age. (b) The scatterplot of the tail decay timescale against the tropical upward mass flux at 70 hPa. The error bars represent the interannual variations of these diagnostics.



**Figure 10.** (a) The fractional contribution of tail to the mean age in the 2000 age spectra (contours) and the differences between the 2080 and 2000 age spectra (color). The tail is defined as the region with transit time older than 4 years. (b) Same as Figure 10a, but for the averaged transit time in the tail region.

no changes in mixing across the subtropical barriers in the middle and upper stratosphere. Thus the tropical pipe becomes more leaky, but only in the base. Mixing decreases significantly just below the tropical pipe and the area of reduced  $\eta$  extends to midlatitudes. Mixing increases in the Arctic lower stratosphere, but it remains the same in the Antarctic stratosphere.

[39] The pattern of changes in  $\eta$  in the tropical/subtropical lower stratosphere indicates that the distribution of  $\eta$  is shifted upward in this region from 2000–2019 to 2080–2099. The upward shift in the mixing pattern is consistent with zonal wind changes. Figure 12 shows the changes in temperature and zonal wind between 2080–2099 and 2000–2019. The meridional temperature gradient increases in the subtropical upper troposphere and lower stratosphere (UTLS), due to strong warming in the tropical upper troposphere. This causes significant westerly acceleration of the zonal wind in the tropical/subtropical UTLS, leading to an upward lift of the subtropical jets and the zero wind line. *Shepherd and McLandress* [2011] showed that, the upward shift of the westerlies in the subtropical lower stratosphere shifts the critical line for wave breaking to higher altitudes, which drives the acceleration of the lower branch of the residual circulation. Since wave breaking results in irreversible mixing, this upward shift of the subtropical jet could also explain changes in mixing in the tropical/subtropical lower stratosphere.

[40] In order to demonstrate the relationship among changes in isentropic mixing, residual circulation, and zonal wind, Figure 13a plots the evolution of the 20-year mean  $\eta$  averaged in  $10^{\circ}$ – $30^{\circ}$  latitudes and 440–520 K against the tropical upward mass flux at 70 hPa and the subtropical UTLS zonal wind averaged in  $10^{\circ}$ – $30^{\circ}$  latitudes and 360–440 K in both hemispheres. The strong correlations among the three diagnostics support our argument that increases in mixing and residual circulation are closely related to each other, and both are driven by zonal wind changes that lead to enhanced wave breaking in the subtropical lower stratosphere.

[41] However, increases of mixing in the subtropical lower stratosphere do not produce older mean age or wider age spectrum widths in this region. Figure 13b shows that as mixing increases, the mean age (black line) and the spectral width (blue line) in the subtropical lower stratosphere decrease. *Ray et al.* [2010] showed that, using the conceptual tropical leaky pipe model, the trend of the mean age is very sensitive to the relative importance of changes in the upwelling and mixing. One important result in this study is that changes in mixing and upwelling are not independent; but are closely related. Our model results indicate that the impact of

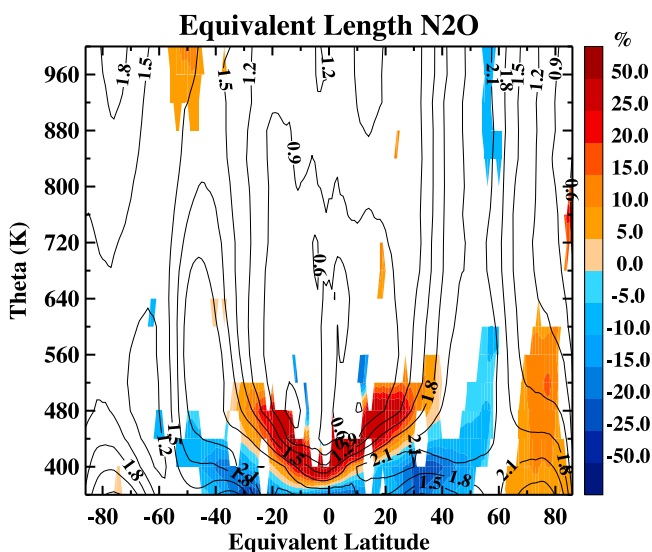


**Figure 11.** Distribution of the normalized equivalent length squared of N<sub>2</sub>O for the period 2000–2019 (contours) and the percentage changes between 2080–2099 and 2000–2019 (color). Only differences statistically significant at the 95% confidence level are shown.

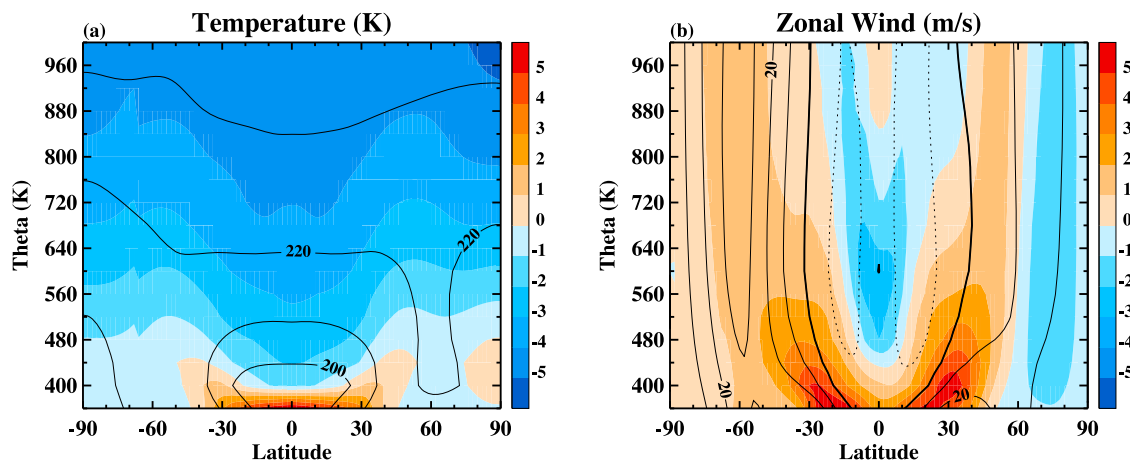


**Figure 12.** (a) Color shadings are differences in temperature between 2080–2099 and 2000–2019. Contours are 2000–2019 mean. (b) Same as Figure 12a, but for the zonal wind.

enhanced mixing on the age spectra is outweighed by the acceleration of the residual circulation.

#### 4.4. Relationship Between Changes in Age Spectra and Chemical Tracers

[42] The mean age of air is compactly related with long-lived chemical tracers such as  $N_2O$  and  $CH_4$  in the lower stratosphere [e.g., Boering *et al.*, 1996]. This compact relationship can be used to infer the distribution of the mean age. For example, Andrews *et al.* [2001] derived an empirical relationship between the mean age and  $N_2O$  in the midlatitude lower stratosphere from NASA ER-2 aircraft measurements. Applying this relationship to all latitudes, they estimated the seasonal distribution of the mean age in the lower stratosphere. However, as the mean age and age spectra change in response to  $CO_2$  increases in the 21st century, the relationship between the mean age and chemical tracers also changes.

[43] Figure 14a compares the compact relationship between the mean age and  $N_2O$  in 2000–2019 and 2080–

2099 in the northern hemisphere lower stratosphere 100–50 hPa. For age older than about 1.5 years, the compact line in 2080–2099 is shifted to the left of the line in 2000–2019. This shift means that the mean age and  $N_2O$  respond differently to circulation change in the 21st century. As the residual circulation speeds up, the isolines of the mean age and long-lived chemical tracers are shifted to higher levels, but the upward shifting in the mean age is stronger such that a given mean age is associated with a smaller mixing ratio of  $N_2O$  in 2080–2099 than in 2000–2019.

[44] The mean age also exhibits a compact relationship with fractional release of CFCs [Schauffler *et al.*, 2003]. The fractional release is defined as  $fr = 1 - \chi(r)/\chi_0$ , where  $\chi(r)$  is the mixing ratio of a CFC at a stratospheric sample region  $r$ , and  $\chi_0$  is the mixing ratio of the same CFC that would have had if there was no chemical loss [Schauffler *et al.*, 2003]. The fractional release provides useful information on photochemical loss of CFCs. Note that when calculating the fractional release,  $\chi_0$  is simply taken as the fixed boundary condition value. But in general when the boundary condition

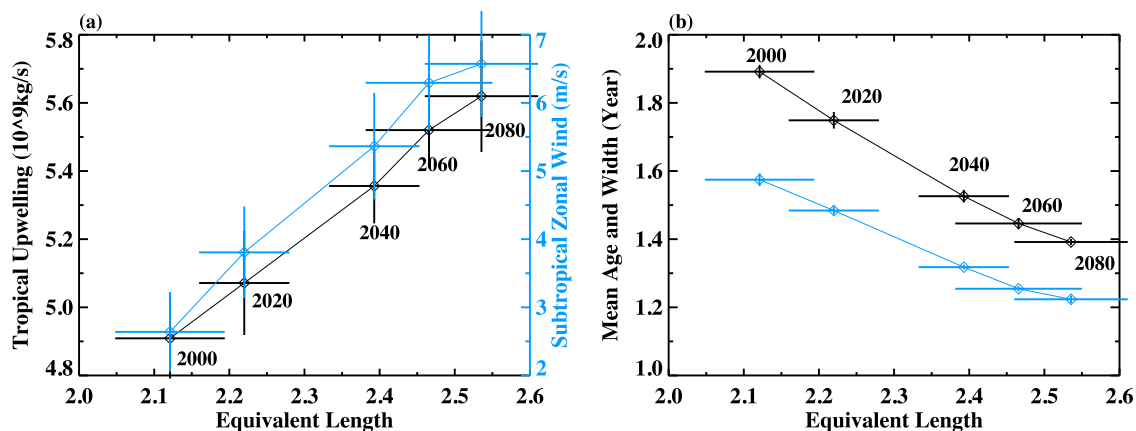


**Figure 13.** (a) The scatterplot of the equivalent length squared of  $N_2O$  in the subtropical lower stratosphere (averaged in  $10^{\circ}$ – $30^{\circ}$  latitudes and 440–520 K) against tropical upward mass flux at 70 hPa (black, left axis), and the scatterplot of the equivalent length squared of  $N_2O$  against the zonal wind in the subtropical UTLS (averaged in  $10^{\circ}$ – $30^{\circ}$  latitudes and 360–440 K, blue, right axis). (b) The scatterplot of the equivalent length squared of  $N_2O$  in the subtropical lower stratosphere against the mean age (black) and spectral width (blue) in the subtropical lower stratosphere (averaged in  $10^{\circ}$ – $30^{\circ}$  latitudes and 70–50 hPa).

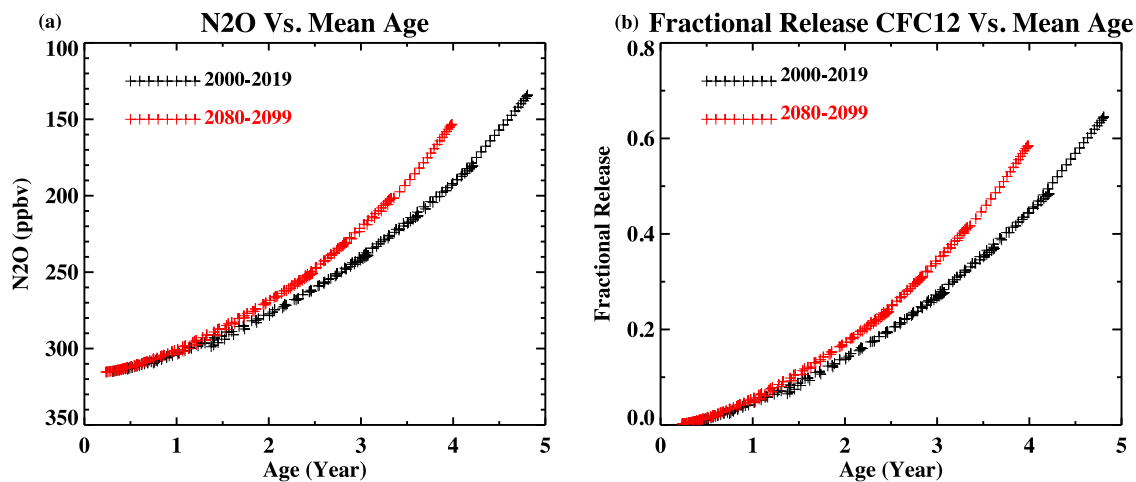


**Figure 14.** (a) Comparison of the compact relationship between the mean age and  $N_2O$  in the northern hemisphere 100–50 hPa between 2000–2019 (black) and 2080–2099 (red). (b) Same as Figure 14a, but for the relationship between the mean age and the fractional release of CFC-12.

changes with time,  $\chi_0$  is calculated using equation (1) with the knowledge of the age spectrum. Figure 14b shows that the compact relationship between the mean age and CFC-12 ( $CF_2Cl_2$ ) changes from 2000–2019 to 2080–2099 in a manner similar to the change of the mean age –  $N_2O$  relationship. Our results are very similar to *Douglass et al.* [2008], who also showed that the GEOSCCM reproduces the observed compact relationship between the mean age and the fractional release. The shift in the relationship between the mean age and the long-lived tracers indicates that the mean age is more sensitive to circulation change than the chemical tracers. We argue that this is because the chemical tracers are less sensitive than the mean age to changes in the tail of the age spectra [*Hall, 2000; Schoeberl et al., 2005*]. The amount of a chemical tracer that has stratospheric sinks at a given location is mainly determined by the fraction of air that has reached above the level where

fast chemistry rapidly destroys the tracer. *Hall* [2000] showed that this fraction is not closely related to the recirculation or the age spectrum tail. Therefore chemical tracers and mean age respond differently to changes in the age spectra.

[45] We use the ideal “radioactive” tracer to help us to better understand why the mean age and long-lived tracers respond differently to circulation change in the 21st century. Assume the radioactive tracer has a spatially uniform decay rate  $\lambda$  in the stratosphere and a fixed surface concentration  $c$ , its mixing ratio can be written as [*Schoeberl et al., 2005*]

$$\chi(r, t) = c \int_0^{\infty} e^{-\lambda\xi} G(r, t | \Omega, t - \xi) d\xi. \quad (3)$$

In contrary to the mean age, the mixing ratio of the radioactive tracer is not sensitive to the tail of the age spectrum.

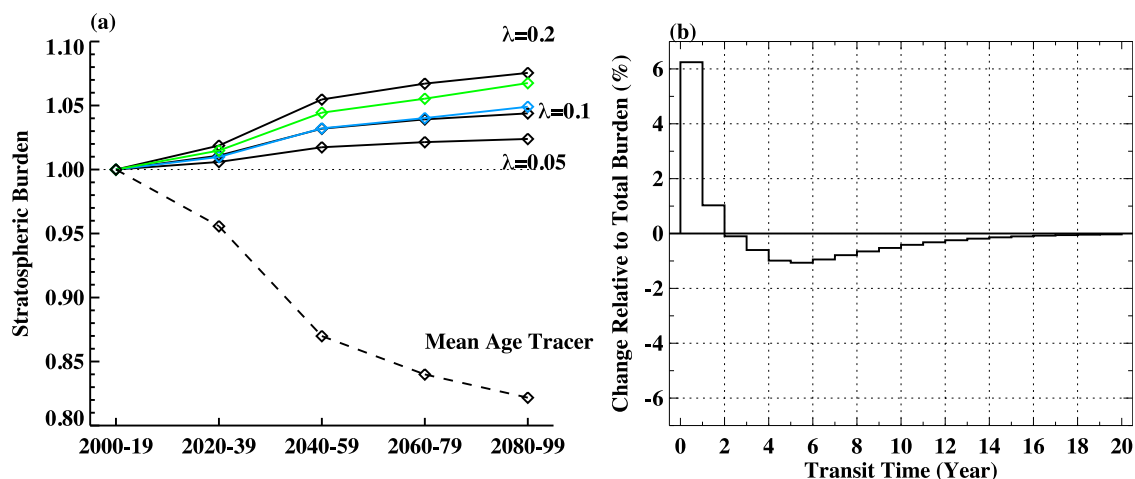


**Figure 15.** (a) Evolution of the stratospheric mass burdens of three radioactive tracers with different decay rates (black solid), the mean age tracer (black dashed), CFC-11 (green) and CFC-12 (blue) in the 21st century relative to their respective 2000–2019 level. (b) Changes of stratospheric air masses between the 2080 and 2000 age spectra relative to the total stratospheric mass burden as a function of transit time at 1-year interval.

Since we have the age spectrum, we can calculate the mixing ratio and the mass burden of the radioactive tracer from equation (3). Figure 15a shows the evolution of the stratospheric (100–1 hPa) mass burdens of three radioactive tracers with different decay rates. For comparison the evolution of the stratospheric burdens of CFC-11 (green), CFC-12 (blue) and the mean age (dashed) are also plotted (recall that CFC-11 and CFC-12 tropospheric mixing ratios are fixed in this simulation). Except for the mean age, all other tracers' relative stratospheric burdens increase in the 21st century. For the radioactive tracers, the faster the decay rate the larger the mass burden increases. The evolution of the stratospheric burdens of CFC-11 and CFC-12 is very similar to the radioactive tracer. The stratospheric burden of CFC-11 increases more than that of the CFC-12 through the 21st century.

[46] Figure 15b shows stratospheric air mass changes between 2080 and 2000 normalized to the total stratospheric mass burden. The stratospheric air mass burden is a constant, but the distribution of air masses of different ages changes with time. Air masses younger than 2 years increase and air masses older than 2 years decrease between 2080 and 2000. The changes of the young and old air masses compensate each other. However, the mass burden of a tracer may increase or decrease with time depending on how the tracer's mixing ratio is weighted by the age spectrum. The mean age, i.e., the mixing ratio of the clock tracer, decreases because the clock tracer is more affected by old air. The radioactive tracers are more sensitive to the changes in the young air than the old air, and the mass burden of the radioactive tracers increases. A radioactive tracer with a faster decay rate has a larger weight in the young air masses than one with a slower decay rate, and therefore its stratospheric burden increases more.

[47] Unlike the radioactive tracer, the loss rates of CFCs (and other chemical tracers) increase rapidly with altitudes. However, the stratospheric burden of CFC-11 and CFC-12 can be approximated by the burden of a radioactive tracer with a decay rate between 0.1 and 0.2 (Figure 15a). Thus we can use the arguments in the previous paragraph to explain changes in the stratospheric burdens of CFC-11 and CFC-12. The increase of the stratospheric burden of CFCs is mainly due to the increase of the residual circulation that affects the first few years of the age spectrum. This result is consistent with *Cook and Roscoe* [2012] who showed that speeding of the residual circulation increases the stratospheric burden of CFC-12 in a simple conceptual model. CFC-11 has a stronger chemical loss rate than CFC-12 [Douglass *et al.*, 2008], and so its stratospheric mass burden increases more than CFC-12. Note that all the above arguments are based on the condition that the tracer's surface boundary condition is fixed. Nevertheless, our analyses clearly show that the age spectrum is more relevant to chemical tracers than the mean age.

## 5. Conclusion

[48] Long-term changes in the stratospheric age spectra in response to CO<sub>2</sub> increases in the 21st century are investigated using a GEOSCCM simulation. We focus on changes in mean age, modal age, spectral width, and age spectrum tail decay timescale. These four timescales characterize different aspects of the age spectra. Model results show that the

mean age, the modal age, the spectral width, and the tail decay timescale all decrease throughout the stratosphere in the 21st century. These changes lead to redistribution of stratospheric air masses at the end of the 21st century: air younger than 2 years increases and air older than 2 years decreases. Our work is the first time that changes in all aspects of age spectra are characterized.

[49] A major purpose of this paper is to identify processes that cause the long-term changes in the mean age of stratospheric air. Two processes are found to be responsible for the decrease of the mean age. The first process is the increase of the residual circulation. This process has been shown to be directly associated with the decrease of the modal age, not the mean age, in the tropical pipe region. The second process is the weakening of the recirculation, which is seen by the decrease of the age spectrum tail and quantified by the decrease of the tail decay timescale. We show for the first time that the weakening of the recirculation plays an important role in the decrease of the mean age. These two processes are closely related to each other, but they impact different aspects of the age spectra. Together they lead to increases of young air masses and decreases of old air masses in the stratosphere, causing the decrease of mean age.

[50] We have also investigated long-term changes in stratospheric mixing using the equivalent length of N<sub>2</sub>O. In the simulation, the tropical pipe becomes more leaky in its base at the end of the 21st century. If there were no changes in tropical upwelling, the enhanced mixing would increase the recirculation between the tropics and midlatitudes, which would lead to older mean age, larger width, and longer tail. However, the increase of isentropic mixing in the subtropical lower stratosphere is closely associated with the increase of tropical upwelling. Our model results indicate that the impacts of increased mixing on the age spectra are dominated by the acceleration of the residual circulation.

[51] The mean age and chemical tracers show different responses to changes in the residual circulation and recirculation. The mean age is heavily weighted by the tail of the age spectrum (recirculation), whereas chemical tracers are more sensitive to the first few years of the age spectrum (residual circulation). Because young and old air masses change differently, the mean age and chemical tracers have different long-term changes in the 21st century. Clearly the age spectrum is more useful than the mean age for the study of trace gases in the stratosphere.

[52] **Acknowledgments.** This work is supported by NASA's Modeling, Analysis and Prediction program. We thank Stacey Frith for data management. Computational resources for this work were provided by NASA's High-Performance Computing through the generous award of computing time at NASA Ames Research Center.

## References

- Andrews, D. G., J. R. Holton, and C. B. Leovy (1987), *Middle Atmosphere Dynamics*, 485 pp., Academic, San Diego, Calif.
- Andrews, A. E., K. A. Boering, S. C. Wofsy, B. C. Daube, D. B. Jones, S. Alex, M. Loewenstein, J. R. Podolske, and S. E. Strahan (2001), Mean ages of stratospheric air derived from in situ observations of CO<sub>2</sub>, CH<sub>4</sub>, and N<sub>2</sub>O, *J. Geophys. Res.*, *106*, 32,295–32,314, doi:10.1029/2001JD000465.
- Austin, J., and F. Li (2006), On the relationship between the strength of the Brewer-Dobson circulation and the age of stratospheric air, *Geophys. Res. Lett.*, *33*, L17807, doi:10.1029/2006GL026867.

- Boering, K. A., S. C. Wofsy, B. C. Daube, H. R. Schneider, M. Loewenstein, J. R. Podolske, and T. J. Conway (1996), Stratospheric mean ages and transport rates from observations of carbon dioxide and nitrous oxide, *Science*, *274*, 1340–1343, doi:10.1126/science.274.5291.1340.
- Butchart, N., and A. A. Scaife (2001), Removal of chlorofluorocarbons by increased mass exchange between the stratosphere and troposphere in a changing climate, *Nature*, *410*, 799–802, doi:10.1038/35071047.
- Butchart, N., et al. (2006), Simulations of anthropogenic change in the strength of the Brewer–Dobson circulation, *Clim. Dyn.*, *27*, 727–741, doi:10.1007/s00382-006-0162-4.
- Butchart, N., et al. (2010), Chemistry-climate model simulations of twenty-first century stratospheric climate and circulation change, *J. Clim.*, *23*, 5349–5374, doi:10.1175/2010JCLI3404.1.
- Cook, P. A., and H. K. Roscoe (2012), Changes in reactive stratospheric gases due to a change in Brewer–Dobson circulation: Results from a simple model, *Atmos. Sci. Lett.*, *13*, 49–54, doi:10.1002/asl.362.
- Douglass, A., R. Rood, S. Kawa, and D. Allen (1997), A three-dimensional simulation of the evolution of the middle latitude winter ozone in the middle stratosphere, *J. Geophys. Res.*, *102*(D15), 19,217–19,232, doi:10.1029/97JD01043.
- Douglass, A. R., R. S. Stolarski, M. R. Schoeberl, C. H. Jackman, M. L. Gupta, P. A. Newman, J. E. Nielsen, and E. L. Fleming (2008), Relationship of loss, mean age of air and the distribution of CFCs to stratospheric circulation and implications for atmospheric lifetimes, *J. Geophys. Res.*, *113*, D14309, doi:10.1029/2007JD009575.
- Ehhalt, D. H., F. Rohrer, S. Schaffler, and M. Prather (2004), On the decay of stratospheric pollutants: Diagnosing the longest-lived eigenmode, *J. Geophys. Res.*, *109*, D08102, doi:10.1029/2003JD004029.
- Engel, A., et al. (2009), Age of stratospheric air unchanged within uncertainties over the past 30 years, *Nat. Geosci.*, *2*, 28–31, doi:10.1038/ngeo388.
- Garcia, R. R., and W. Randel (2008), Acceleration of the Brewer–Dobson circulation due to increases in greenhouse gases, *J. Atmos. Sci.*, *65*, 2731–2739, doi:10.1175/2008JAS2712.1.
- Garcia, R. R., D. R. Marsh, D. E. Kinnison, B. A. Boville, and F. Sassi (2007), Simulation of secular trends in the middle atmosphere, 1950–2003, *J. Geophys. Res.*, *112*, D09301, doi:10.1029/2006JD007485.
- Garcia, R. R., W. J. Randel, and D. E. Kinnison (2011), On the determination of age of air trends from atmospheric trace species, *J. Atmos. Sci.*, *68*, 139–154, doi:10.1175/2010JAS3527.1.
- Haine, T. W. N., H. Zhang, D. W. Waugh, and M. Holzer (2008), On transit-time distributions in unsteady circulation models, *Ocean Modell.*, *21*, 35–45, doi:10.1016/j.ocemod.2007.11.004.
- Hall, T. M. (2000), Path histories and timescales in stratospheric transport: Analysis of an idealized model, *J. Geophys. Res.*, *105*, 22,811–22,823, doi:10.1029/2000JD900329.
- Hall, T. M., and R. A. Plumb (1994), Age as a diagnostic of stratospheric transport, *J. Geophys. Res.*, *99*, 1059–1070, doi:10.1029/93JD03192.
- Hall, T. M., D. W. Waugh, K. A. Boering, and R. A. Plumb (1999a), Evaluation of transport in stratospheric models, *J. Geophys. Res.*, *104*, 18,815–18,839, doi:10.1029/1999JD900226.
- Hall, T. M., D. J. Wuebbles, K. A. Boering, R. S. Eckman, J. Lerner, R. A. Plumb, D. H. Rind, C. P. Rinsland, D. W. Waugh, and C.-F. Wei (1999b), Transport experiments, in *Models and Measurements Intercomparison II*, edited by J. H. Park et al., *Rep. NASA/TM-1999-209554*, pp. 110–189, NASA, Hampton, Va.
- Holzer, M., I. G. McKendry, and D. A. Jaffe (2003), Springtime trans-Pacific atmospheric transport from east Asia: A transit-time probability density function approach, *J. Geophys. Res.*, *108*(D22), 4708, doi:10.1029/2003JD003558.
- Intergovernmental Panel on Climate Change (IPCC) (2001), *Climate Change 2001: The Scientific Basis. Contribution of Working Group I to the Third Assessment Report*, edited by J. T. Houghton et al., Cambridge Univ. Press, New York.
- Li, F., J. Austin, and J. Wilson (2008), The strength of the Brewer–Dobson circulation in a changing climate: Coupled chemistry-climate model simulations, *J. Clim.*, *21*, 40–57, doi:10.1175/2007JCLI1663.1.
- Li, F., D. Waugh, A. R. Douglass, P. A. Newman, S. Pawson, R. S. Stolarski, S. E. Strahan, and J. E. Nielsen (2012), Seasonal variations of stratospheric age spectra in GEOSCCM, *J. Geophys. Res.*, *117*, D05134, doi:10.1029/2011JD016877.
- Ma, J., D. W. Waugh, A. R. Douglass, S. R. Kawa, and S.-J. Lin (2003), Evaluation of the transport in the Goddard Space Flight Center three-dimensional chemical transport model using the equivalent length diagnostic, *J. Geophys. Res.*, *108*(D6), 4201, doi:10.1029/2002JD002268.
- McLandress, C., and T. G. Shepherd (2009), Simulated anthropogenic changes in the Brewer–Dobson circulation, including its extension to high latitudes, *J. Clim.*, *22*, 1516–1540, doi:10.1175/2008JCLI2679.1.
- Nakamura, N. (1996), Two-dimensional mixing, edge formation, and permeability diagnosed in an area coordinate, *J. Atmos. Sci.*, *53*, 1524–1537, doi:10.1175/1520-0469(1996)053<1524:TDMFEA>2.0.CO;2.
- Neu, J. L., and R. A. Plumb (1999), Age of air in a “leaky pipe” model of stratospheric transport, *J. Geophys. Res.*, *104*, 19,243–19,255, doi:10.1029/1999JD900251.
- Oman, L., D. W. Waugh, S. Pawson, R. S. Stolarski, and P. A. Newman (2009), On the influence of anthropogenic forcings on changes in the stratospheric mean age, *J. Geophys. Res.*, *114*, D03105, doi:10.1029/2008JD010378.
- Pawson, S., R. S. Stolarski, A. R. Douglass, P. A. Newman, J. E. Nielsen, S. M. Frith, and M. L. Gupta (2008), Goddard Earth Observing System chemistry climate model simulations of stratosphere ozone temperature coupling between 1950 and 2005, *J. Geophys. Res.*, *113*, D12103, doi:10.1029/2007JD009511.
- Prather, M. J. (1996), Time scales in atmospheric chemistry: Theory, GWP for CH<sub>4</sub> and CO, and runaway growth, *Geophys. Res. Lett.*, *23*, 2597–2600, doi:10.1029/96GL02371.
- Ray, E. A., et al. (2010), Evidence for changes in stratospheric transport and mixing over the past three decades based on multiple data sets and tropical leaky pipe analysis, *J. Geophys. Res.*, *115*, D21304, doi:10.1029/2010JD014206.
- Reithmeier, C., R. Sausen, and V. Grewe (2008), Investigating lower stratospheric chemical transport: Lagrangian calculation of mean age and age spectra in the GCM ECHAM4, *Clim. Dyn.*, *30*, 225–238, doi:10.1007/s00382-007-0294-1.
- Rienecker, M. M., et al. (2008), The GEOS-5 data assimilation system—Documentation of versions 5.0.1, 5.1.0, and 5.2.0, *NASA Tech. Memo., NASA TM-2008-104606*, vol. 27, 118 pp.
- Schaffler, S. M., E. L. Atlas, S. G. Donnelly, A. Andrews, S. A. Montzka, J. W. Elkins, D. F. Hurst, P. A. Romashkin, G. S. Dutton, and V. Stroud (2003), Chlorine budget and partitioning during the Stratospheric Aerosol and Gas Experiment (SAGE) III Ozone Loss and Validation Experiment (SOLVE), *J. Geophys. Res.*, *108*(D5), 4173, doi:10.1029/2001JD002040.
- Schoeberl, M. R., A. R. Douglass, Z. Zhu, and S. Pawson (2003), A comparison of the lower stratospheric age spectra derived from a general circulation model and two data assimilation systems, *J. Geophys. Res.*, *108*(D3), 4113, doi:10.1029/2002JD002652.
- Schoeberl, M. R., A. R. Douglass, B. Polansky, C. Boone, K. A. Walker, and P. Bernath (2005), Estimation of stratospheric age spectrum from chemical tracers, *J. Geophys. Res.*, *110*, D21303, doi:10.1029/2005JD006125.
- Schoeberl, M. R., A. R. Douglass, R. S. Stolarski, S. Pawson, S. E. Strahan, and W. Read (2008), Comparison of lower stratospheric tropical mean vertical velocities, *J. Geophys. Res.*, *113*, D24109, doi:10.1029/2008JD010221.
- Shepherd, T. G. (2002), Issues in stratosphere-troposphere coupling, *J. Meteorol. Soc. Jpn.*, *80*, 769–792, doi:10.2151/jmsj.80.769.
- Shepherd, T. G., and C. McLandress (2011), A robust mechanism for strengthening of the Brewer–Dobson circulation in response to climate change: Critical-layer control of subtropical wave breaking, *J. Atmos. Sci.*, *68*, 784–797, doi:10.1175/2010JAS3608.1.
- SPARC CCMVal (2010), SPARC CCMVal report on the evaluation of chemistry-climate models, edited by V. Eyring, T. G. Shepherd, and D. W. Waugh, *SPARC Rep. 5*, WMO, Geneva, Switzerland. [Available at <http://www.atmosph.physics.utoronto.ca/SPARC/>]
- Strahan, S. E., M. R. Schoeberl, and S. D. Steenrod (2009), The impact of tropical recirculation of polar composition, *Atmos. Chem. Phys.*, *9*, 2471–2480, doi:10.5194/acp-9-2471-2009.
- Strahan, S. E., et al. (2011), Using transport diagnostics to understand chemistry climate model ozone simulations, *J. Geophys. Res.*, *116*, D17302, doi:10.1029/2010JD015360.
- Waugh, D. W., and T. M. Hall (2002), Age of stratospheric air: Theory, observations, and models, *Rev. Geophys.*, *40*(4), 1010, doi:10.1029/2000RG000101.
- Waugh, D. W., S. E. Strahan, and P. A. Newman (2007), Sensitivity of stratospheric inorganic chlorine to differences in transport, *Atmos. Chem. Phys.*, *7*, 4935–4941, doi:10.5194/acp-7-4935-2007.
- World Meteorological Organization (2007), Scientific assessment of ozone depletion: 2006, *Global Ozone Res. Monit. Project Rep. 50*, 572 pp., Geneva, Switzerland.